New Sensing Method for Cartridge Valves

Massimiliano Ruggeri[1*], Sara Baldoni[2], Chiara Gialluca[2], Christopher Rosi[2], Matteo Ferri[3], Luca Belsito[3]

1. CNR - STEMS, via Canal Bianco, 28 – 44124 Ferrara, Italy
2. VIS Hydraulics S.r.l. Innovation Center, Via G. Marconi, 115, 41028 Serramazzoni (MO) Italy
3. CNR – ISMN, Via Piero Gobetti 101, 40129 Bologna, Italy
** corresponding author, massimiliano.ruggeri@cnr.it*

Abstract.

Trends in hydraulic system design tend to avoid proportional valves because of energy losses intrinsic to their operation. Yet valves are fundamental in many applications and often are used in functional safety critical applications. Current systems require increasing precision in controls and actuations, as well as higher safety performance levels in both components and systems. Both of these requirements involve sensors to make the component and systems fully observable and controllable. It is particularly difficult to implement sensors integrated directly in cartridge valves. However, sensors installed directly inside the valves would allow direct observation of their behaviour. This would provide highly valuable diagnostic information from functional safety perspective and would be crucial for precise control of valve operation. The paper presents a new sensor integration method for cartridge valves, which allows a direct observation of their functionality and enables a precise tuning of the valve in low flow metering condition, as well as the direct control of valve safe position. The applied sensor is a miniaturized MEMS sensor whose usage is the consequence of a mechanical-electronic valve co-design approach. The valve design, the sensor and its readout electronics, as well as the tests are presented, with a discussion of the possible usage of the assembly and a more general idea for new design of both proportional and status valves.

Keywords. Cartridge Valve, Proportional Valve, Pressure Sensing, Functional Safety, Valve Diagnosis, Sensors, MEMS, DETF.

1. INTRODUCTION

The increasing demand for compact, high-performance fluid power systems has driven significant research toward the integration of miniaturized sensors directly within hydraulic components, particularly valves [1]. Miniaturized pressure sensors represent an important focus of this research. In conventional hydraulic systems, pressure sensing is typically performed using externally mounted transducers connected via ports or tubing, which introduces delays, parasitic volumes, and measurement uncertainty. Recent advances in Micro-Electro-Mechanical Systems (MEMS) technology have enabled the development of pressure sensors with dimensions on the order of millimetres or below, opening the possibility of true in-situ sensing within valve bodies and flow passages. MEMS devices leverage micro-machined silicon structures—such as membranes, beams, or cavities—to transduce pressure into electrical signals via piezoresistive, capacitive, or resonant mechanisms and, to date, piezoresistive sensing has remained the dominant approach due to its robustness and compatibility with industrial environments [2]. Resonant MEMS sensors represent an alternative approach offering significantly higher strain sensitivity and excellent long-term stability.

State-of-the-art miniaturized pressure sensors typically achieve footprints below 1–2 mm and thicknesses below 0.1 mm, enabling integration into confined geometries such as micro-channels, catheter tips, or embedded cavities [3].

Advanced designs employ membrane-based architectures, where pressure-induced deformation is measured through integrated strain gauges or piezoresistive films. More recent developments include integrated microchannel sensors, in which the sensing element is fabricated directly adjacent to or within the fluid path, minimizing dead volume and improving dynamic response [4]. These approaches are particularly relevant for hydraulic valves, where accurate measurement of transient pressure gradients across small control volumes is critical for performance characterization and control using both absolute and differential pressure sensors [5].

A key trend in the literature is the move toward fully embedded sensing architectures, where the sensing element is structurally integrated into the component rather than mounted as a discrete device. This includes chip-level integration using techniques such as flip-chip bonding [6], through-silicon vias, or wafer-level packaging, allowing the sensor to be embedded within metallic or polymeric housings while maintaining electrical connectivity and environmental isolation. In harsh environments such as hydraulic systems, the sensing element is typically protected by a metallic or polymeric isolation diaphragm, enabling exposure to high-pressure fluids while shielding sensitive electronics. These packaging strategies are essential to ensure compatibility with high pressure levels, temperature variations, and aggressive media typical of fluid power applications.

Emerging research further explores ultra-miniaturized and high-sensitivity sensing technologies, including devices based on two-dimensional materials (e.g., $PtSe_2$ or graphene membranes), which exhibit significantly enhanced sensitivity due to reduced mass and increased gauge factors. Such sensors demonstrate the potential for sub-millimeter, high-resolution pressure measurement, although their application in hydraulic environments remains largely at the research stage [7]. Additionally, multifunctional micro-sensors capable of simultaneously measuring pressure, temperature, and flow are being developed, offering the prospect of integrated diagnostic capabilities within a single embedded device [8]. Despite these advances, several challenges remain for the adoption of embedded pressure sensors in hydraulic valves. These include reliable sealing under high pressure (often exceeding 250–300 bar), vibration resistance, long-term stability in oil-contaminated environments, thermal drift compensation, and the integration of signal conditioning electronics within limited space. Consequently, while MEMS-based miniaturized sensors have demonstrated strong potential for embedded valve sensing, their widespread industrial implementation is still constrained by packaging, robustness, and cost considerations. Nevertheless, ongoing developments in microfabrication, materials, and system integration indicate that fully sensorized hydraulic valves, with pressure sensing embedded directly within the valve body, represent a key direction for next-generation fluid power systems.

Pressure is one of the most important parameters to measure in hydraulic systems, but both for flow prediction and for functional safety concerns, valve spool position sensing is still one of the most critical embedded measurements; indeed most sensors are integrated but not fully embedded (often mounted externally on valve body) and not miniaturized enough [9]. For that reason several studies focus on valve spool position inference through EMC analysis as shown in [10] or innovative approach to valve actuation design through piezo-electric devices integrating piezo-electric sensors for spool movement sensing [11].

Finally, functional safety requirements ask for higher diagnosability both indirect, through virtual sensors and software, and direct, through real sensors. For that reason, there are many studies to infer valve faults, even using machine learning, like the one in [12], in which sensing the current in the coil, both spool stuck and spring failure valve faults can be identified. From the direct diagnosis side, many studies attempt, with a multi-sensor approach and a sensor fusion, to make diagnosis and predictive diagnosis of valves [13]. But the crux of these studies is the need for high sampling frequencies to perform the Fast Fourier Transform (FFT) of the signals and evaluate the remaining useful life of the components.

Valve diagnosis and, in particular, faults of its core is a key point for functional safety, due to the need to understand if valves are in their safe position, and that diagnosis is also made through different sensors like accelerometers for an indirect sensing of the core position [14]. Unfortunately, these methods do not also include the possibility of improving the control of the valve spool position.

2. THE MEMS-DETF SENSOR

The type of MEMS used in this research is a double-ended tuning fork (DETF) type MEMS developed by CNR from 2012 and published in [15], [16] and [17], and now in production through a spin-off company. It is based on a micro-mechanical tuning fork structure connected to micro capacitors vibrating in vacuum inside the MEMS chip.

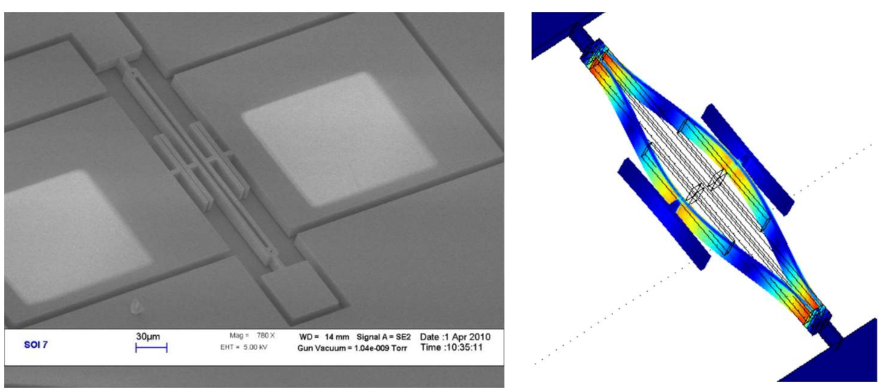

Figure 1. MEMS-DETF structure (left) and working principle (right)

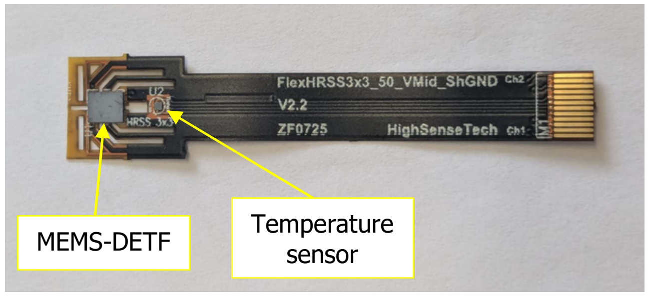

Figure 2. MEMS-DETF and MEMS Temperature Sensor mounted on flat cable

The tuning fork is maintained in continuum vibration at its resonance frequency through an external electronic circuit in the readout electronics connected to the MEMS chip pinout. The tuning fork is connected to the MEMS chip at its ends and when the chip is subjected to strain, then the tuning fork changes its resonance frequency according to the strain. If the strain is a compressive strain, then the frequency becomes lower, while if the strain is an extensive strain, then the resonance frequency increases. This frequency shift is linear with the strain. Due to the high stiffness of silicon, it shows a very high sensitivity of ~ 200 pε, 10.000 times the sensitivity of a traditional flexible strain gauge. This characteristic together with the possibility to vary the sample frequency (until 10-15 kHz) by changing the buffer size of frequency values, corresponding to each MEMS oscillation, used to calculate the frequency in the microcontroller's reciprocal frequency counter peripheral, make the sensor particularly suitable for hydraulic applications. Of greatest interest are those applications in which it is difficult to find a position where to install a traditional sensor, or where a high sample frequency is required. The MEMS-DETF has been applied to hydraulic components through years and published in [18], [19] and [20]. In this work the sensor has been applied to a valve for the first time.

3. VALVE WORKING PRINCIPLE

The valve used in this project is manufactured by VIS Hydraulics, and the technical code is PFR0.S08, represented with its hydraulic symbol in Figure 3.

Figure 3. Proportional flow regulator and its hydraulic symbol

This is a non-pressure compensated proportional flow regulator, equipped with a solenoid, designed to control the amount of oil flowing between port 2 (inlet port) and port 1 (outlet port), in response to a specific current applied to the solenoid.

As shown in Figure 4, by regulating the current applied to the solenoid, it is possible to regulate the flow between the minimum and the maximum admitted values.

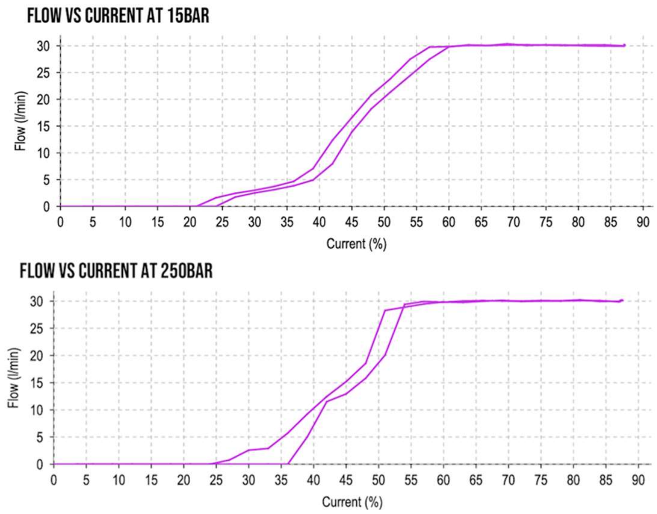

Figure 4. flow regulation curves at different pressure drops

The current flowing through the coil generates an electromagnetic field that magnetizes the internal elements, and an attraction force is generated between the so-called moving plunger and the fixed armature, leading to an internal movement of the pilot and main poppet. By changing the current value, the attraction force changes accordingly, and a different opening point is reached, thus obtaining a different regulated flow. Because the valve is not pressure compensated, the amount of the regulated flow in response to the current may change depending on the pressure variation across the inlet and outlet ports.

As shown in Figure 5, the original valve is modified by creating an internal pressure chamber (called sensing chamber), designed to withstand the same pressure acting on the internal stage. The pressure in the sensing chamber is detected by the MEMS sensor applied in the modified nut.

In the real case, something happens inside the valve, which can be divided in three stages:

- Coil off: the valve is closed and there is no oil flow between inlet and outlet port, and the pressure inside the valve (and in the sensing chamber) is equal to the inlet pressure, as showed in Figure 6.
- Coil on with current between 20% and 60% of the steady-state current: when the electromagnetic force generated by the electromagnetic field acting on the moving plunger is sufficient to start to open the axial orifice, the main poppet lifts itself, reaching an equilibrium position with a certain distance from the pilot poppet. By

increasing the current, this distance is maintained (so both the main and the pilot poppet lifts together with the increasing magnetic force inside the pole tube).

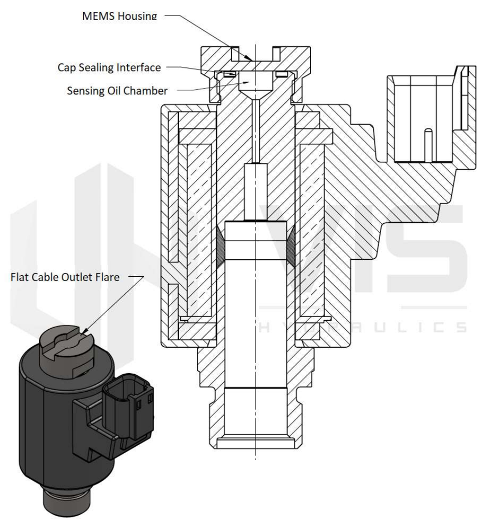

Figure 5. New valve design with the sensing chamber

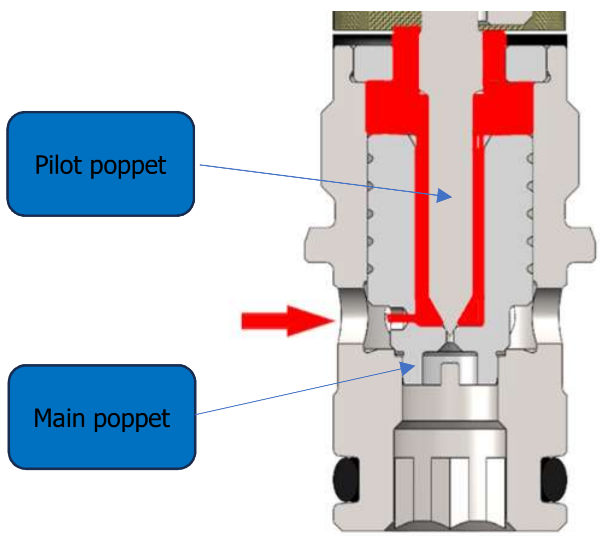

Figure 6. internal pressure level @ 0 A current

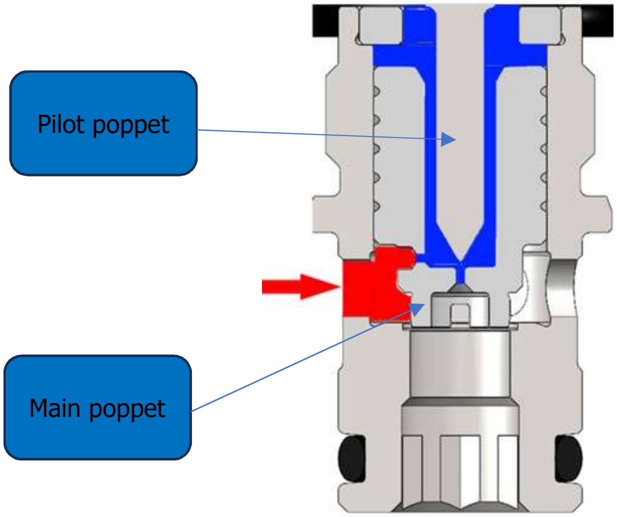

Figure 7. Internal pressure level at intermediate current.

The pressure inside the sensing chamber is no longer the inlet one (Figure 7), but now there is an intermediate pressure that can be described by r recalling the turbulent flow equation through a restrictor, derived from the Bernoulli equation:

$$Q = C_d \cdot A \cdot \sqrt{2 \cdot \frac{\Delta p}{\rho}} \tag{1}$$

where Q is the flow, C_d is the efflux coefficient, A is the orifice area, Δp is the pressure drop across the orifice, and ρ is the fluid density.

At equilibrium, neglecting the leakages it can be assumed that the flow across the radial orifice is the same as the flow across the axial one, and under steady-state conditions we can neglect some terms, obtaining the following equation:

$$C_d \cdot A_{in}\sqrt{p_{in} - p_{ch}} = C_d \cdot A_{out}(x) \cdot \sqrt{p_{ch} - p_{out}} \tag{2}$$

Where, in our case, the inlet area is related to a fixed radial orifice, while the outlet area is given by a percentage of the area of the axial orifice, depending on the distance between the pilot and the main poppet.

From simulations, we know that the intermediate position of the pilot poppet opens around the 40% of the outlet area; with this assumption, the pressure in the sensing chamber can be approximated, obtaining:

$$p_{ch} = \frac{A_{03}^2 \cdot p_{in} + A_{04}^2 \cdot p_{out}}{A_{04}^2 + A_{03}^2} \tag{3}$$

For the valve under study:

- With an inlet pressure of 200 bar, the internal calculated pressure is around 133 bar.

- With an inlet pressure of 100 bar, the internal calculated pressure is around 67 bar.
- With an inlet pressure of 50 bar, the internal calculated pressure is around 33 bar.

More generally a linear dependency from p_{in} and p_{out} can be plotted and the result for p_{out} 1, 10, 50 and 80 bar is shown in Figure 8.

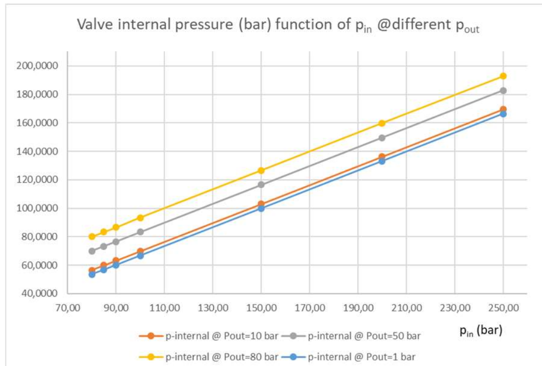

Figure 8. Internal pressure function of p_{in} (inlet) and p_{out} (load)

- Coil on with current above the 65% of the steady-state current. Now the electromagnetic force is sufficiently high to pull up the plunger and the pilot poppet, while the main poppet reaches its maximum stroke; this leads to the complete valve opening, and the pressure inside drops to the minimum value that is usually the p_{out}, the load pressure. In this condition the maximum pressure drop of the valve is reached, around 14 bar in the test bench where the p_{out} is the reservoir pressure. In other condition in real applications the pressure is related to the p_{out}, the pressure of the load.

4. TEST SETUP

The sensor was glued on the cap (Figure 9 left) using the Micro Measurements M Bond AE-10 epoxy and it was thermally conditioned in order to stabilize the glue for higher temperatures. Then the cap was mounted on the valve pole tube, facing the sensing chamber. Then the valve was mounted on a special three-way manifold. A first setup was prepared at the static test bench to verify the sensor sensitivity in respect to the pressure strain in the sensing chamber (Figure 9 right). The main objective of the test was to qualitatively verify that the sensor was able to acquire pressure transients with sufficient resolution with respect to the variation of the resonance frequency with respect to the pressure variation.

To evaluate the sensor performance a program application under Windows was created. The program communicates with the sensor readout electronics control unit through the USB 3.0 connection and it permits acquiring at high speed all the data from the sensor, allowing the complete acquisition of the raw data.

The observed response during various tests with 30 bar steps and 50 bar steps, respectively, manually generated in the bench, was that the sensor and its double ended tuning fork sensing elements inside were capable of acquiring the pressure variation. In particular, due to the asymmetrical shape of the cap, the Sensor 1 (Channel 1 in yellow in Figure 9), directed in the same axis as the machining created to position the sensor in a protected position, by removing material from the cylindrical cap, is more sensitive than Sensor 2 (Channel 2 in green in Figure 9). Sensor 2 is aligned along the axis orthogonal to the aforementioned mechanical machining.

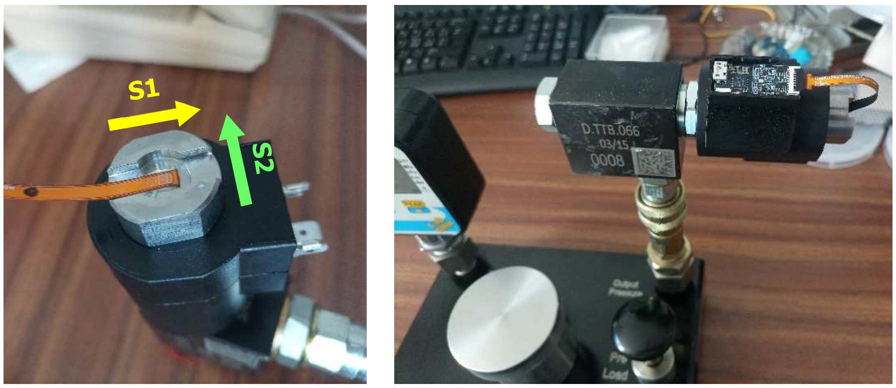

Figure 9. The sensor glued on the cap (left) and the valve at the static pressure test bench (right)

- The greater presence of material therefore makes the cap more rigid in the direction orthogonal to the machining, making the tuning fork less sensitive in that same direction. From a quantitative point of view, allowing for small measurement errors in data collected manually during the tests, it can be stated that Sensor 2 is approximately one-third less sensitive compared to Sensor 1.

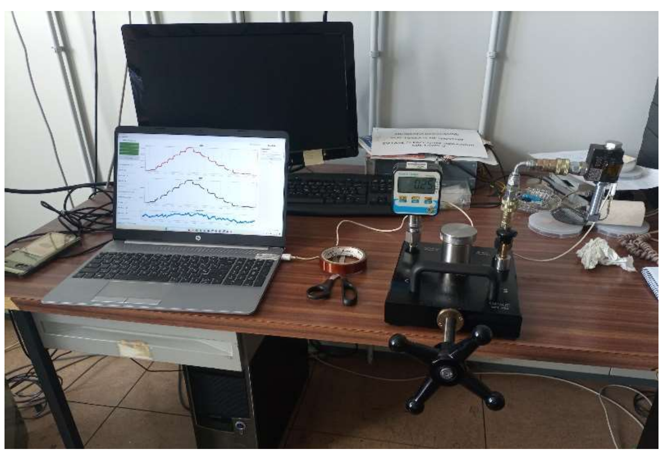

Figure 10. The static test bench (manual pressure regulation bench) and the application program for resonance frequency acquisition. Valve is mounted without coil.

Specifically, the data collected indicate an average sensitivity of:

- Channel 1: 62.2 Hz/bar;

- Channel 2: 41.4 Hz/bar.

Such data can be easily obtained from graphs such as the one shown in the Figure 11, which are obtained from the data recorded by the PC application that records the data communicated in real time by the sensor via USB communication. In the test shown in the graph in Figure 11, steps of 50 bar from around 1.5 bar to 300 bar are manually generated using the static pressure bench. In the test the resonance frequency of both sensors, together with the component temperature, is acquired in real time and stored for post processing, here made through Excel after conversion of the CSV data files.

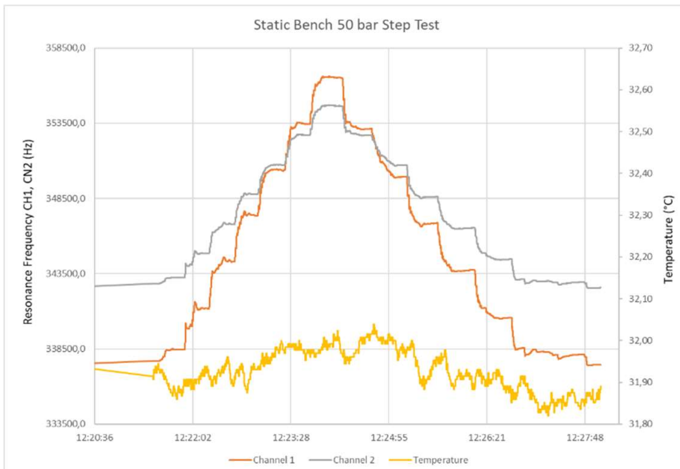

Figure 11. 50 bar steps test at static pressure test bench

In order to evaluate the sensor's resolution with respect to the variation in Hz per bar, as a comparison it can be used the resolution obtainable from a standard reciprocal frequency counter of a modern microcontroller, which allows acquisition of tenths of a Hz even with data of hundreds of kHz. Therefore, the resolution that Sensor 1 can achieve is greater than 0.002 bar and the Sensor 2 a resolution greater than 0.003 bar.

5. SENSOR QUALIFICATION AT TEST BENCH

To have a complete test qualification both in static and dynamic conditions, a test campaign was planned and executed at the Innovation Centre premises of the VIS Hydraulics Company. The valve was mounted on the test bench and connected to both the inlet and outlet ports in the same configuration used in actual machine applications (Figure 12). It is a proportional flow control valve, whose regulated flow rate depends both on the force transmitted by the coil to the spool and on the inlet pressure, therefore is of the uncompensated type. Therefore, acquiring the inlet pressure in real time could be a very interesting feature for the electronic control of the valve. The first test was designed to verify whether the sensor is able to acquire the inlet pressure when this pressure is returned to the sensing chamber created inside the valve, near the sensorized cap (see Figure 5 for reference).

The first test was performed maintaining the valve unpowered in the closed position, which can be critical due to the need for the pressure to be returned in the sensing chamber at the end of pole tube. Pressure steps were generated at the test bench and the sensor signals were acquired during the test. As shown in the upper plot of Figure 13, the sensors signal is changing according to the pressure generated by the test bench (lower plot of Figure 13). Moreover, the resonance frequency steps are proportional to the pressure steps, due to the screwed cap strain under the pressure in the sensing chamber.

Figure 12. The valve with the sensor and the readout electronics at test bench

As it can be seen in the figure, the resonance frequency levels are not the same at the beginning and end of the test, despite the initial and final pressures being equal. This is due to the temperature difference between the valve and the cap, which is detected by the MEMS temperature sensor in the flat cable adjacent to the MEMS-DETF strain sensor. This effect, which has a significant impact on the measurement, results from the thermal deformation of the metal component. This deformation is essentially linear with temperature and can be compensated for using two possible methods: a temperature-dependent strain ratio parameter between silicon and metal, or by detecting the change in resonance frequency due to thermal deformation.

In the case under study it was found that the thermal strain is around F_T= 3235,8 Hz/°C. This temperature compensation was then applied to the acquired sensors resonance frequencies starting from the initial test temperature using the simple equation:

$$f_{corr}(t) = f(t) - F_T * (T(t) - T(t_0)) \quad (4)$$

where f_{corr} is the compensated resonance frequency, f is the uncompensated resonance frequency, F_T is the thermal strain frequency correction factor, T(t) is the current temperature and $T(t_0)$ is the initial temperature of the test. The result of the compensation is presented in Figure 14. In the Figure, the resonance frequency levels at the beginning and the end of the test, corresponding to the same pressure levels, are the same, validating the accurate temperature compensation made through (4).

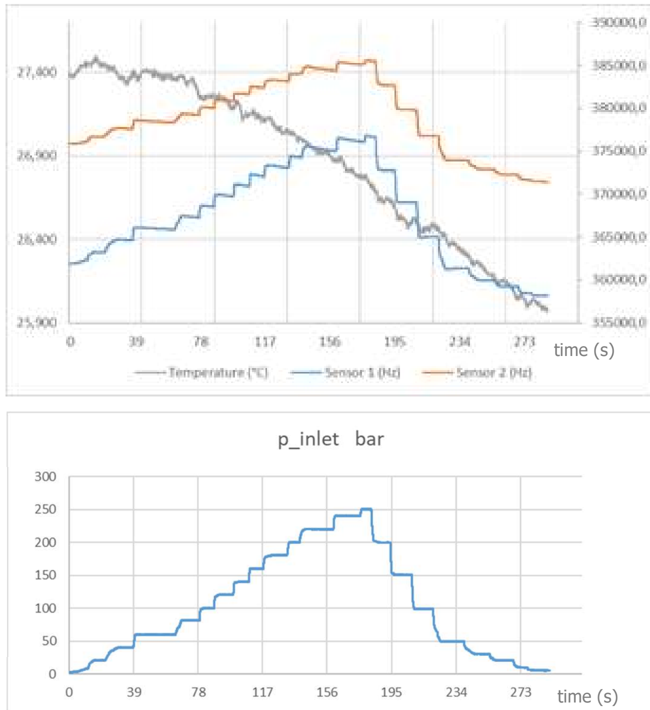

Figure 13. Uncompensated Sensor Response to the Pressure steps at Test Bench

In order to understand the relationship between the sensor signals and the real pressure values acquired through the sensors installed in the test bench, a comparison is made with a test where 50 bar steps of the test bench pressure were generated both increasing and decreasing pressure from 9 bar to 250 bar.

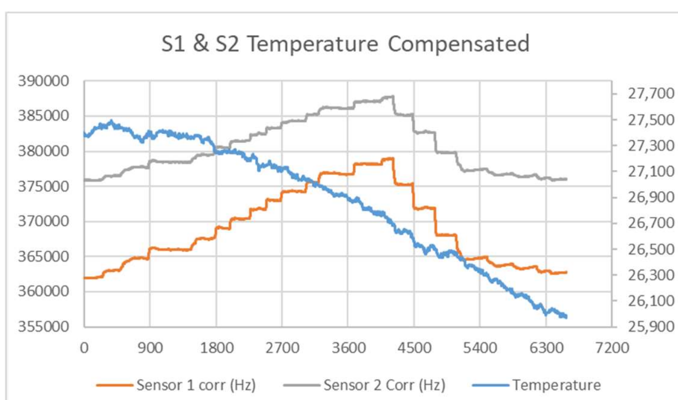

Figure 14. Temperature Compensated Sensor Response to the Pressure

A Matlab® script was used to adapt both the scale and the timing of the acquisitions. The sensor signal is compensated in temperature and the timing is shifted in order to make the starting time of both acquisitions synchronized with the pressure steps. The result is shown in Figure 15.

The pressure estimated from the raw MEMS resonance-frequency signal was compared with the reference pressure measured by the inline pressure sensor. The MEMS frequency was converted into pressure using a linear calibration derived from the mean values measured during the static pressure plateaus. The calibration yielded a scale factor of 0.0120 bar/Hz, corresponding to a MEMS pressure sensitivity of approximately 83.3 Hz/bar. To minimize the influence of possible time-synchronization errors between the two acquisition systems, only the static pressure conditions were considered, excluding the transition regions. The reconstructed MEMS pressure shows good agreement with the reference measurement, with an RMSE of 1.157 bar, corresponding to 0.461% of the full-scale pressure range.

In fact, as it can be noted in the figure, the MEMS-DETF sensor is capable of acquiring pressure values with excellent agreement with the data from the sensors used in the test bench.

The final result of the test is that the sensor installed in the screwed cap allows measuring the inlet pressure, which is returned to the sensing chamber obtained in the terminal position of the valve's pole tube.

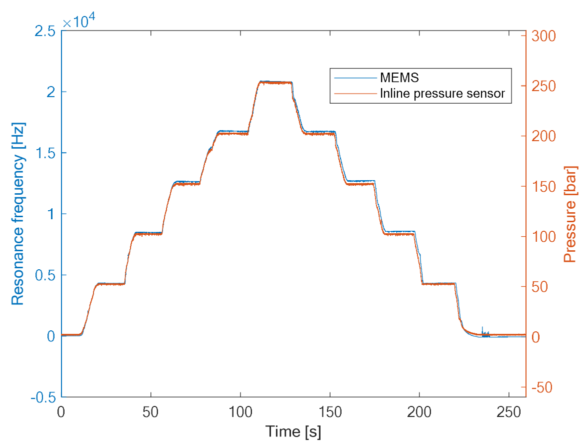

Figure 15. Temperature Compensated Sensor Response (normalized) to the Pressure Steps test

In order to complete the sensor qualification it is fundamental to understand what happens to the internal pressure when the valve is commanded and then the plunger changes its position, consequently the pilot poppet and main poppet change their positions accordingly.

6. Functional Tests: Internal Pressure Observer

Once it was demonstrated that the sensor facing the internal sensing chamber is capable of acquiring the inner pressure with excellent agreement with the test bench sensors, subsequent tests were performed at the same test bench, by testing the valve under all its operating conditions. Electrical commands were generated for the valve to power the coil and activate the valve's internal spool, causing it to open proportionally to the command. The tests were repeated at different circuit supply pressures (p_{in}), in order to verify the general applicability and the repeatability of the functionality tested.

A test setup was created where the valve was controlled using a production electronic board usually sold together with the valve. The board, connected with a PC application through a CAN network using a CAN to USB gateway, is capable both to program, to calibrate and to control the valve output, also generating repeatable timed commands. Indeed the system is also used for endurance tests in the company facilities. A PWM ramp and the corresponding current ramp were generated from 0% to 100% and way back, in order to replicate an entire cycle of valve command from valve fully closed to valve fully open and then the opposite transient until valve fully closed condition. The test was repeated at different inlet pressure (p_{in}) values, in order to validate the sensor signal. Here the results for p_{in} = 100 bar and p_{in} = 200 bar are presented.

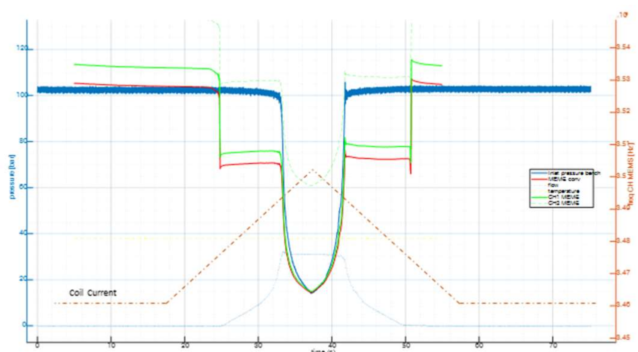

Figure 16. Full Valve Cycle at p_{in} = 100 bar

As it can be observed in Figure 16 for the test at p_{in}=100 bar, the control cycle lasts 40 seconds, that means that it is a quasi-static test, because the dynamics are very limited.

In the test diagram it can be observed both the line pressure and the MEMS signals, as well as the oil flow through the valve and the command to the valve coil (coil real current).

- The first behaviour that can be noticed is that the internal pressure is not equal to Inlet pressure p_{in} from the instant the poppet starts moving, as explained in the valve working principle discussion.
- The second behaviour that can be noticed is that the internal pressure remains constant from the first moment of valve opening in metering conditions until saturation opening. Practically speaking the internal pressure holds a nearly constant value across the entire flow regulation range and its value is near the theoretical one of 67 bar calculated for 100 bar of inlet pressure (red line in the figure, corresponding to the temperature compensated MEMS signal).
- The third behaviour that can be noticed is that when the valve is fully open the internal pressure becomes equal to the sum of the load pressure and the pressure difference across the valve (p_{load} + Δp).

The test case at p_{in} = 200 bar is presented in Figure 17. As it can be observed in the figure, the behaviour of the valve under coil actuation is the same as in the previous case. The difference in this case is that the equivalent internal pressure measured by the MEMS sensor in the regulation phase is around 133-135 bar, a value completely compatible with the value previously calculated in equation (3).

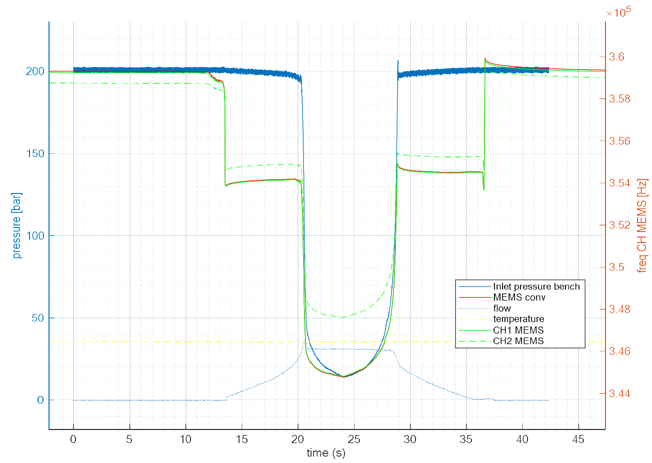

Figure 17. Full Valve Cycle at p_{in} = 200 bar

Another interesting result to be noticed is that the valve opens at different current values due to pressure and this event is not directly observable without the MEMS-DETF sensor. Conversely, the automatic control could be used to acquire the change in internal pressure and could regulate the metering phase of the valve control depending on the current and the boundary conditions; this would ensure repeatability of the command regardless of the valve's operating conditions.

7. CONCLUSION

The MEMS-DETF sensor installed in the screwed cap of the cartridge valve, facing the sensing chamber, where the internal valve pressure is reported, demonstrates some important aspects of valve sensor-oriented design. The sensor further demonstrates its capability of being used as an external pressure sensor in hydraulic applications applicable to thick walls due to its high sensitivity. The mechanical-electrical co-design of the valve demonstrates that a combined approach to design enables the development of new components with higher diagnosability rate and easier to control precisely, due to new sensor integration methods. The sensor applied to cartridge valves is a powerful element for both control and diagnostics. Moreover, it allows the precise metering control, even if the valve is uncompensated. Indeed it is able to detect the exact force - and relative coil current - at which the valve spool starts to move. From the diagnosis point of view, it allows a direct observation of the effects of the valve spool (and poppet) movement. Based on the internal valve pressure acquisition and its relationship with the inlet pressure measurement, it is possible to evaluate the status of the valve. This allows determining whether the valve is closed, partially open for flow regulation, or fully open. Furthermore, it can also be used as a redundant pressure sensor due to the proven relationship between the Inlet pressure and the valve internal pressure. The information on the status of the valve is crucial for functional safety critical applications, where the safe state is often related to the de-energized position of a safety valve (e.g. load dump) and/or to a position of a proportional valve, to prevent both single critical failures and latent faults. The next steps in studying the potential applications of these promising MEMS-DETF sensors in valves, involve an innovative approach to valve design, aiming to create areas and volumes where all the pressures involved in valve control can be measured. The ultimate goal will be the design of a fully integrated valve with the sensors required for its complete control.

8. REFERENCES

[1] Liu, J., Yuan, C., Matias, L., Bowen, C., Dhokia, V., Pan, M. and Roscow, J. (2024), Sensor Technologies for Hydraulic Valve and System Performance Monitoring: Challenges and Perspectives. Adv. Sensor Res., 3: 2300130. https://doi.org/10.1002/adsr.202300130.

[2] Song P, Ma Z, Ma J, Yang L, Wei J, Zhao Y, Zhang M, Yang F, Wang X. Recent Progress of Miniature MEMS Pressure Sensors. Micromachines. 2020; 11(1):56. https://doi.org/10.3390/mi11010056.

[3] W. Hasenkamp, D. Forchelet, K. Pataky, J. Villard, H. Van Lintel, A. Bertsch, Q. Wang, P. Renaud, Polyimide/SU-8 catheter-tip MEMS gauge pressure sensor, 2012, Biomedical Microdevices, № 5, p. 819-828, Springer Science and Business Media LLC, doi: 10.1007/s10544-012-9661-8.

[4] M. Dijkstra, M.J. de Boer, J.W. Berenschot, T.S.J. Lammerink, R.J. Wiegerink, M. Elwenspoek, Miniaturized thermal flow sensor with planar-integrated sensor structures on semicircular surface channels, Sensors and Actuators A: Physical, Volume 143, Issue 1, 2008, Pages 1-6, ISSN 0924-4247, https://doi.org/10.1016/j.sna.2007.12.005.

[5] Fan, Xutao et al. "A High-Performance Micro Differential Pressure Sensor." Micromachines 2024, 15(11), 1396; https://doi.org/10.3390/mi15111396.

[6] Huang M, Wu X, Zhao L, Han X, Xia Y, Gao Y, Cui Z, Zhang C, Yang X, Qiao Z, Li Z, Han F, Yang P, Jiang Z. Small-size temperature/high-pressure integrated sensor via flip-chip method. Microsyst Nanoeng. 2024 Jul 23;10:104. doi: 10.1038/s41378-024-00723-3. PMID: 39050588; PMCID: PMC11266362.(integrated pressure and temperature sensor)

[7] Zhou Y, Werner EM, Lee E, Chu M, Nguyen T, Costa KD, Hui EE, Khine M. High-resolution integrated piezoresistive sensors for microfluidic monitoring. Lab Chip. 2021 Jan 7;21(1):83-92. doi: 10.1039/d0lc01046d. Epub 2020 Dec 10. PMID: 33300516; PMCID: PMC9521707.

[8] Chi-Yuan Lee, Chen Chia-Hung, Chin-Lung Hsieh, Chong-An Jiang, Siao-Yu Chen, Flexible, Multifunctional Micro-Sensor Applied to Internal Measurement and Diagnosis of Vanadium Flow Battery, Micromachines; Basel Vol. 13, Fasc. 8, (2022): 1193. doi:10.3390/mi13081193.

[9] M. Papoutsidakis, A. Srivastava and S. Chowdhary, Displacement Sensors for Linear Electrical, Hydraulic and Pneumatic Actuators, 2019 Amity International Conference on Artificial Intelligence (AICAI), Dubai, United Arab Emirates, 2019, pp. 269-273, doi: 10.1109/AICAI.2019.8701227.

[10] Wilber Acuña-Bravo, Enrico Canuto, Marco Agostani, Marco Bonadei, Proportional electro-hydraulic valves: An Embedded Model Control solution, Control Engineering Practice, Volume 62, 2017, Pages 22-35, ISSN 0967-0661, doi 10.1016/j.conengprac.2017.01.013.

[11] Šimic M, Herakovič N. Investigation of Innovative High-Response Piezoelectric Actuator Used as Smart Actuator–Sensor System. Applied Sciences. 2024; 14(18):8523. https://doi.org/10.3390/app14188523.

[12] BN, P., Yelchuri, H., Shastry, V., & Prabhakar, T. V. (2022). PreMa: predictive maintenance of solenoid valve in real-time at embedded edge-level. arXiv preprint arXiv:2211.12326.

[13] Li X, Zhang L, Tan T, Wang X, Zhao X, Xu Y. Multi-Sensor Data Fusion and Vibro-Acoustic Feature Engineering for Health Monitoring and Remaining Useful Life Prediction of Hydraulic Valves. Sensors (Basel). 2025 Oct 11;25(20):6294. doi: 10.3390/s25206294. PMID: 41157348; PMCID: PMC12568100.

[14] Z. Wang, W. Li, C. Feng, B. Qiu and X. Lu, "Hydraulic Valve Core Fault Diagnosis Applied with a Data-driven Approach," 2025 IEEE International Instrumentation and Measurement Technology Conference (I2MTC), Chemnitz, Germany, 2025, pp. 1-6, doi: 10.1109/I2MTC62753.2025.11079224.

[15] M. Ferri, F. Mancarella, L. Belsito, A. Roncaglia, J. Yan, A. A. Seshia, K. Soga, J. Zalesky, “Strain sensing on steel surfaces using vacuum packaged MEMS resonators”, Procedia Eng., vol. 5, pp. 1426–1429, Jan. 2010.

[16] L. Belsito, M. Ferri, F. Mancarella, A. Roncaglia, J. Yan, A. A. Seshia, K. Soga, “High-resolution strain sensing on steel by Silicon-On-Insulator flexural resonators fabricated with chip-level vacuum packaging”, in Proc. 17th Int. Conf. Solid-State Sens. Actuators Microsyst., Barcelona, Spain, Jun. 2013, pp. 992–995.

[17] L. Belsito, M. Ferri, F. Mancarella, L. Masini, J. Yan, A. A. Seshia, K. Soga, A. Roncaglia , “Fabrication of high-resolution strain sensors based on wafer-level vacuum packaged MEMS resonators”, Sens. Actuators A, Phys., vol. 239, pp. 90–101, Mar. 2016.

[18] M. Ruggeri, G. P. Massarotti, L. Belsito, A. Roncaglia, Indirect Pressure Measurement on Hydraulic Components Through New MEMS Strain Sensors, ASME/BATH 2017 Symposium on Fluid Power and Motion Control, doi. 10.1115/FPMC2017-4355.

[19] G.P. Massarotti, C. Ferrari, E. Codina Macia and M. Ruggeri. “General Lecture: Mems Sensors In Hydraulics, An Opportunity To Create Smart Components.” (2020), 12th International Fluid Power Conference (12. IFK). Dresden, October 12 – 14, 2020. https://doi.org/10.25368/2020.114.

[20] M. Ruggeri, L. Belsito, F. Bosi, P. Cominetti, M. Ferri, M. Ferri, A. Roncaglia, Advancements in Noninvasive Pressure Sensing in Hydraulic Components, ASME/BATH 2023 Symposium on Fluid Power and Motion Control, Sarasota FL, November 2023, doi:10.1115/FPMC2023-109140.